Macromolecules

ARTICLE

pubs.acs.org/Macromolecules

Two Different Uniplanar−Axial Orientations of Syndiotactic Polystyrene Films

Alexandra R. Albunia, Paola Rizzo,* and Gaetano Guerra

Dipartimento di Chimica e Biologia and INSTM Research Unit, Università degli Studi di Salerno, Via Ponte don Melillo, 84084, Fisciano, Italy

ABSTRACT: Two different kinds of uniplanar−axial orientations, exhibiting the polymer chain axis parallel to the main draw direction (c_{ax})and the ac plane parallel or perpendicular with respect to the film plane ($a_{\parallel}c_{ax}$ and $a_{\perp}c_{ax}$, respectively) have been achieved for several cocrystalline s-PS phases. The preparation procedures involve an unbalanced biaxial stretching, leading to mesomorphic trans-planar phases, followed by cocrystallization procedures induced by suitable guest molecules. In particular, cocrystalline films with $a_{\parallel}c_{ax}$ and $a_{\perp}c_{ax}$ orientations have been obtained by using more (e.g., carbon disulfide) and less volatile (e.g., 1,4-dimethylnaphthalene) guest molecules. These uniplanar−axial orientations can be maintained after guest removal procedures leading to the δ phase (i.e., the crystalline phase exhibiting nanoporous cavities), after thermal treatments, leading to the orthorhombic dense γ phase. These uniplanar−axial orientations after chloroform sorption−desorption procedures lead to $a_{\perp}c_{ax}$ and $b_{\perp}c_{ax}$ orientations of the orthorhombic nanoporous ε phase (i.e., the crystalline phase exhibiting channel-shaped porosity). High degrees of uniplanar−axial orientations can lead to a complete 3-D orientational order among the crystallites and as a consequence maximize the anisotropy of the physical properties.

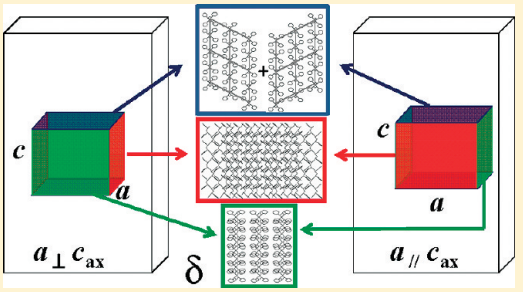

INTRODUCTION

For semicrystalline polymers, since covalent bonding is stronger than the interchain interactions, the primary slip direction is generally along the chain axis. Hence, uniaxial stretching procedures lead to the typical *axial* orientation, with the crystalline *c* axis preferentially parallel to the stretching direction.

For biaxial stretching, beside the slip direction, also a primary slip plane generally determines the final crystal texture.[1] In polymers with no specific intermolecular interactions (such as hydrocarbon polymers), molecular shape and packing density play major roles in determining the slip planes. For instance, for poly(ethylene-terephtalate) (PET) the slip plane is parallel to the phenyl rings.[1,2] For hydrocarbon polymers, for which the only interchain interactions are of van der Waals type, the primary slip plane is generally that one containing the chain axis and having the highest density. This, for instance, occurs for the monoclinic α form of i-PP, whose primary slip plane is the highest density (0*k*0) plane,[3a−d] that is the plane defined by the crystallographic *a* and *c* axes.[4]

For biaxial stretching, with equal draw ratios in two perpendicular directions, polymers generally develop an *uniplanar* orientation,[1−3] that is the primary slip plane tends to become parallel with respect to the film plane. For biaxial stretching, with different draw ratios in the two perpendicular directions, polymers generally develop an *uniplanar−axial* orientation,[1−3] that is the primary slip plane tend to become parallel with respect to the film plane while the chain axes tend to become parallel to the main draw direction.

As for s-PS films, by cocrystallization with suitable low-molecular-mass guest molecules,[5] it is possible to achieve the unprecedented formation of three different kinds[6] of uniplanar orientations, which correspond to the three simplest orientations of the high planar-density *ac* layers (i.e., layers of close-packed alternated enantiomorphous s-PS helices that characterize most s-PS cocrystalline phases) with respect to the film plane. These three uniplanar orientations have been named $a_{\parallel}c_{\parallel}$, $a_{\parallel}c_{\perp}$ and $a_{\perp}c_{\parallel}$, indicating crystalline phase orientations presenting the *a* and *c* (chain) axes parallel (∥) or perpendicular (⊥) to the film plane.[6h] The degree and the kind of uniplanar orientation depends on the selected technique (solution crystallizations or solvent induced crystallizations or recrystallizations) as well as on the chemical nature of the guest.[6] The three uniplanar orientations (without substantial loss of their degree of orientation) are maintained after guest extraction procedures leading to the δ phase,[7] as well as after thermal annealing procedures[6b,d,e] leading to the dense helical γ phase,[8] and subsequent chloroform treatment procedures leading to the nanoporous channeled ε phase.[9] In the latter case, the three uniplanar orientations correspond to the *a*, *b*, or *c* orthorhombic axes preferentially perpendicular to the film surface.[6i] It is also worth adding that some orientational order can be maintained also after crystal-to-crystal transitions involving chain conformation changes from the helical to the zigzag planar. In fact, suitable thermal treatments on s-PS films

Received: April 7, 2011
Revised: June 6, 2011
Published: June 22, 2011

Scheme 1. Schematic Representation of Biaxially Drawn sPS Films[a]

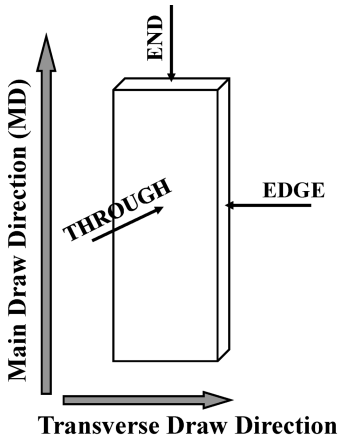

[a] MD is the main draw direction, and TD is the transverse draw direction. Diffraction experiments have been conducted by using X-ray beam perpendicular to the film surface (THROUGH) or parallel to the transverse direction (EDGE) or parallel to the main draw direction (END).

presenting the three different *uniplanar* orientations of their helical crystalline phases can lead to films with *planar* orientations of their zigzag planar α[10] and β[11] crystalline phases.[6b] In particular, crystalline phases with their chain axes preferentially perpendicular or parallel to the film surface, can be obtained.[6b−d]

The availability of crystalline and cocrystalline s-PS films with three different kinds of uniplanar orientation has allowed establishing fine structural features, like, e.g., experimental evaluation of the orientation of transition moment vectors of host and guest vibrational modes, with respect to the host chain axes.[12] It has allowed active guest orientation control[13] for cocrystalline films that have been proposed as advanced optical (e.g., fluorescent and photoreactive),[14] electric,[15] and magnetic[16] materials. Moreover, for the δ nanoporous phase, the three different kinds of uniplanar orientation have been shown to be helpful to control guest diffusivity.[17]

In this contribution we show that biaxial stretching procedures on amorphous s-PS films, followed by suitable guest-induced cocrystallization, can lead to two different kinds of uniplanar−axial orientations, exhibiting axial orientation of the chain axis (crystalline *c* axis) and uniplanar orientation of the *ac* plane ($a_{\parallel}c_{\parallel}$ or $a_{\perp}c_{\parallel}$). For the sake of simplicity, these $a_{\parallel}c_{\parallel}$-uniplanar/*c*-axial and $a_{\perp}c_{\parallel}$-uniplanar/*c*-axial orientations will be simply named $a_{\parallel}c_{ax}$ and $a_{\perp}c_{ax}$ respectively, where "ax" indicates parallel to the main draw direction while ∥ and ⊥ indicate parallel and perpendicular to the film plane.

EXPERIMENTAL SECTION

Materials and Preparation Procedures. The s-PS used in this study was manufactured by Dow Chemical Company under the trademark Questra 101. The ^{13}C nuclear magnetic resonance characterization showed that the content of syndiotactic triads was over 98%. The weight-average molar mass obtained by gel permeation chromatography (GPC) in trichlorobenzene at 135 °C was found to be $M_w = 3.2 \times 10^5$ with the polydispersity index, $M_w/M_n = 3.9$.

Pure solvents were purchased from Aldrich and used without further purification.

Amorphous unoriented s-PS films, having a thickness of 100−150 μm, were obtained by melt extrusion at 300 °C with an extrusion head of 200 mm × 0.5 mm. These amorphous films were stretched by following two different procedures. Films were uniaxially stretched at strain rate of 0.16 s^{-1}, at a draw ratio of λ (final length/initial length) ≈ 3.3, in the temperature range 105−110 °C with a dynamometer INSTRON 4301. Films were biaxially stretched at strain rate of 0.1 s^{-1}, in the temperature range of 105−110 °C, with a Brükner stretching machine. The draw ratio along the main and the transverse draw directions was of λ ≈ 3.3 and 1.6, respectively (see scheme1).

The stretched films were crystallized leading to cocrystalline phases, by immersion in pure solvents generally at room temperature, by immersion in 1,4-dimethylnaphthalene (DMNP) and decalin at 50 °C and by exposition to carbon disulfide (CS_2) vapors for 3 days at room temperature.

Syndiotactic polystyrene δ form films with both $a_{\parallel}c_{ax}$ and $a_{\perp}c_{ax}$ uniplanar−axial orientations were obtained from s-PS cocrystalline films, after guest removal from cocrystalline phases, by immersion in acetonitrile for 3 h. In all cases, 100 min of desorption at room temperature was sufficient to remove the acetonitrile. The residual guest content in the samples, after these extraction procedures, as evaluated by thermogravimetric measurements, was lower than 0.1%.

Syndiotactic polystyrene γ form films with both uniplanar−axial orientations were obtained by annealing of the corresponding nanoporous δ form samples at 160 °C for 2 h. Syndiotactic polystyrene ε forms films with both uniplanar−axial orientations were obtained by treatment with chloroform of γ form films, in turn obtained by annealing of δ form samples at 130 °C, followed by guest desorption by immersion in acetonitrile for 3 h.

All the prepared films showing uniplanar−axial orientations, exhibiting cocrystalline or δ, or γ, or ε phases, present a degree of crystallinity in the range 30−45%, as determined by the Fourier transform infrared method described in ref 18.

The solvents used to induce cocrystallization in s-PS films have been compared on the basis of their volatility (boiling point and vapor pressure at 20 °C) and mainly on the basis of their ability in inducing the formation of the corresponding s-PS cocrystalline phases. In particular, a cocrystallization kinetic index (I_C) has been evaluated by FTIR measurements based on the intensity of the helical crystalline peak at 572 cm^{-1}, as induced by 30 min of room temperature solvent sorption in s-PS α form films (having a thickness of 150 μm, as obtained by annealing of the nanoporous δ form samples at 210 °C for 1 h). The index I_C has been assumed to be equal to 0 and 1 when this helical crystalline peak is absent and fully developed, respectively.

Characterization Techniques. Wide-angle X-ray diffraction patterns (with nickel filtered Cu Kα radiation) were obtained, in transmission, by using a cylindrical camera (radius =57.3 mm). The patterns were recorded on a BAS-MS imaging plate (FUJIFILM) and processed with a digital imaging reader (FUJIBAS 1800). In particular, to recognize the kind of crystalline phase orientation, photographic X-ray diffraction patterns were taken by having the X-ray beam perpendicular to the film surface (THROUGH) or parallel to the transverse direction (EDGE) or parallel to the main draw direction (END) (see Scheme 1) and by placing the film sample parallel to the axis of the cylindrical camera. Wide-angle X-ray diffraction patterns were also obtained, in reflection, with an automatic Bruker diffractometer.

Infrared spectra were obtained in wavenumber range 400−4000 cm^{-1} at a resolution of 2.0 cm^{-1} with a Vertex 70 Bruker spectrometer equipped with deuterated triglycine sulfate (DTGS) detector and a Ge/KBr beam splitter. The frequency scale was internally calibrated to 0.01 cm^{-1} using a He−Ne laser. 32 scans were signal averaged to reduce the noise. Polarized infrared spectra were recorded by use of a SPECAC 12000 wire grid polarizer.

The degree of uniplanar orientation of a crystal plane exhibiting *hkl* Miller indexes (f_{hkl}), with respect to the film plane, has been formalized on a quantitative numerical basis using Hermans' orientation function:[19]

$$f_{hkl} = (3\,\overline{cos^2\,x_{hld}} - 1)/2 \quad (3)$$

by assuming $\overline{\cos^2 x_{hkl}}$ as the average cosine squared values of the angle, x_{hkl}, between the normal to the film surface and the normal to the (*hkl*) crystallographic plane.

If the direction normal to the *hkl* plane is unique (i.e., there are no other equivalent directions in the crystal),[19a] f_{hkl} is equal to +1 or −0.5 when the (*hkl*) crystallographic planes of all crystallites are perfectly parallel or perpendicular to the film plane, respectively. For the case of random orientation f_{hkl} is equal to zero.

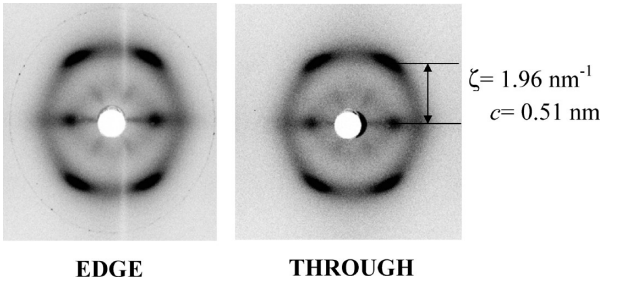

Figure 1. X-ray diffraction patterns of a biaxially stretched film with $\lambda_{\parallel}$ = 3.3 and $\lambda_{\perp}$ = 1.6, taken by having the X-ray beam perpendicular to the film surface (THROUGH) or parallel to the transverse direction (EDGE) and by placing the film sample parallel to the axis of the cylindrical camera. The distance between the equator and the first layer line allows one to establish the along the chain periodicity of 0.51 nm.

The quantity $\overline{\cos^2 x_{hkl}}$ has been experimentally evaluated, by the above-described END X-ray diffraction patterns, as:

$$\overline{cos^2\,x_{hkl}} = \overline{cos^2\,\chi_{hkl}} = \frac{\int_0^{\pi/2} I(\chi_{hkl})\,cos^2\,\chi_{hkl}\,sin\,\chi_{hkl}\,d\chi_{hkl}}{\int_0^{\pi/2} I(\chi_{hkl})\,sin\,\chi_{hkl}\,d\chi_{hkl}} \quad (4)$$

where $I(\chi_{hkl})$ is the intensity distribution of a (*hkl*) diffraction on the Debye ring and χ_{hkl} are the azimuthal angles measured from the horizontal or vertical lines of END patterns like those of Figures 2 and 3.

The diffracted intensities $I(\chi_{hkl})$ of eqs 2 and 4 were obtained by using an AFC7S Rigaku automatic diffractometer (with monochromatic Cu Kα radiation), and were collected sending the X-ray beam parallel to the film surface and parallel to the main stretching direction, recorded on a BAS-MS imaging plate (FUJIFILM) and processed with a digital imaging reader (FUJIBAS 1800).

The degree of orientation of the chain axes of the crystalline phases with respect to the stretching direction has been evaluated on the basis of polarized infrared spectra.

In particular, it has been used the axial orientation factor:[20]

$$f_{c,IR} = S\frac{(2\,cot^2\,\theta + 2)}{(2\,cot^2\,\theta - 1)} \quad (1)$$

where S is the order parameter:

$$S = \frac{(R-1)}{(R+2)} \quad (2)$$

and $R = A_{\parallel}/A_{\perp}$ is the dichroic ratio, $A_{\parallel}$ and $A_{\perp}$ being the measured absorbance for electric vectors parallel and perpendicular to the draw

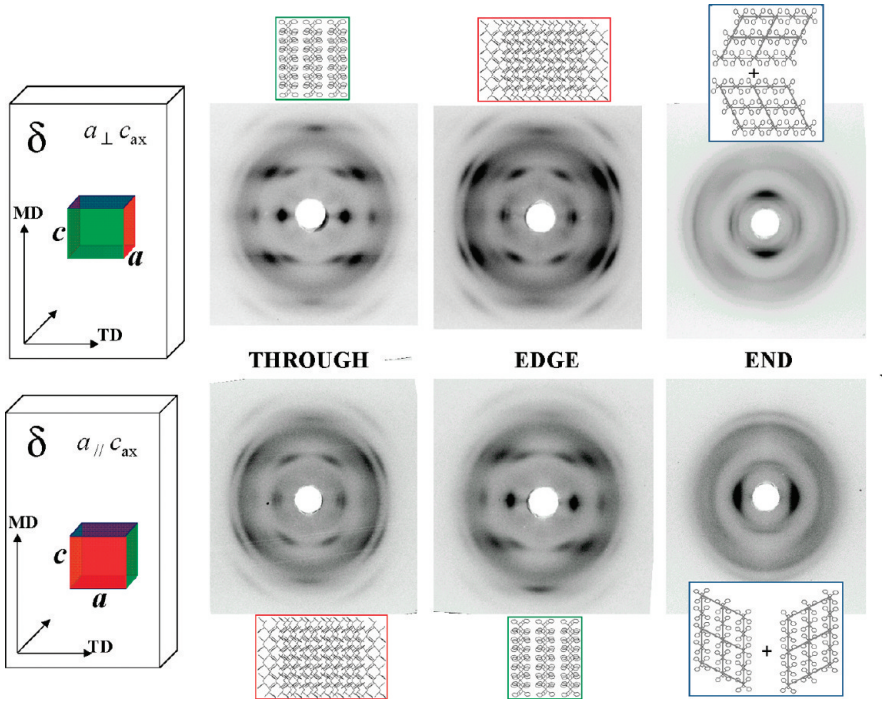

Figure 2. Photographic X-ray diffraction patterns, as taken by having the X-ray beam perpendicular to the film surface (THROUGH) or parallel to the transverse direction (EDGE) or parallel to the main draw direction (END) (see Scheme 1), of the biaxially stretched film of Figure 1 after guest-induced cocrystallization, followed by guest removal, leading to the nanoporous δ phase: (lower part) cocrystallization induced by CS_2, leading to the $a_{\parallel}c_{ax}$ uniplanar−axial orientation; (upper part) cocrystallization induced by DMNP, leading to the $a_{\perp}c_{ax}$ uniplanar−axial orientation. The scheme on the left shows the preferential orientation of the unit cell with respect to the draw directions and to the film plane. The models above and below the photographic patterns show the view normal to the X-ray beam, for the two ideal uniplanar−axial orientations.

dx.doi.org/10.1021/ma200806x |*Macromolecules* 2011, 44, 5671–5681

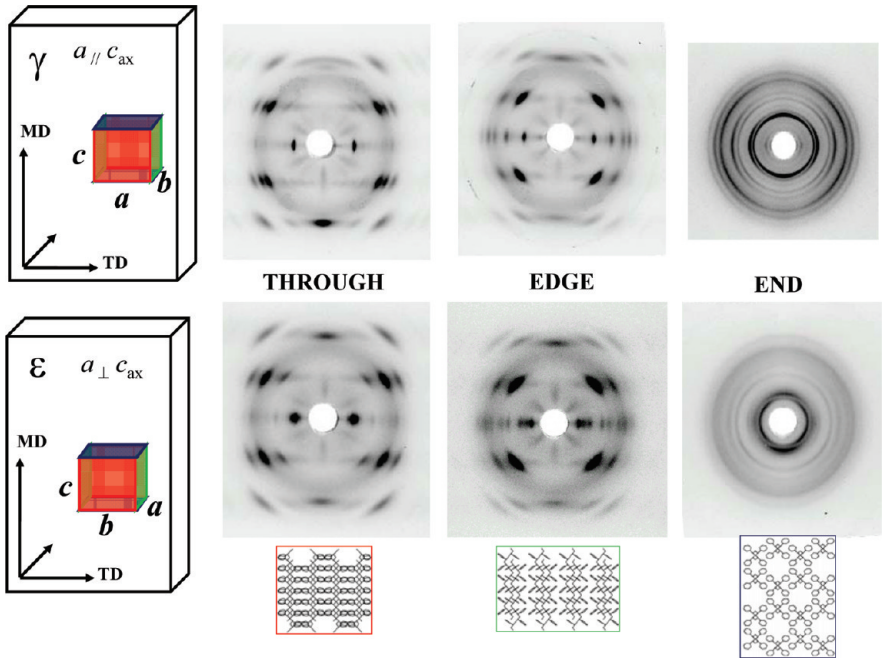

Figure 3. Photographic X-ray diffraction patterns, as taken by having the X-ray beam perpendicular to the film surface (THROUGH) or parallel to the transverse direction (EDGE) or parallel to the main draw direction (END) (see Scheme 1), of the biaxially stretched film of Figure 2 after thermal treatment leading to the γ phase with $a_{\parallel}c_{ax}$ uniplanar−axial orientation (upper part), after thermal treatment and subsequent sorption and desorption of chloroform, leading to the ε phase with $a_{\perp}c_{ax}$ uniplanar−axial orientation (lower part). The scheme on the left shows the preferential orientation of the unit cells with respect to the draw directions and to the film plane. The models below the photographic patterns of the ε form film show the view normal to the X-ray beam, for the ideal $a_{\perp}c_{ax}$ uniplanar−axial orientation.

direction respectively, and θ being the angle between the chain axis and the transition moment vector of the vibrational mode. For the helical δ phase the orientation factor $f_{c,IR}$ has been evaluated by the dichroic ratio of the 572 cm^{-1} infrared peak. Both peaks are characterized by transition moment vectors parallel to the chain axes ($\theta = 0°$).[12,13] This orientation factor is equal to 1 for perfect alignment, whereas it is equal to −0.5 for perpendicular alignment and zero for random orientation.

RESULTS AND DISCUSSION

Preparation and Characterization by X-ray Diffraction of Films with $a_{\parallel}c_{ax}$ and $a_{\perp}c_{ax}$ Uniplanar−Axial Orientations. X-ray diffraction patterns of a biaxially stretched film with $\lambda_{\parallel} = 3.3$ and $\lambda_{\perp} = 1.6$, taken by having the X-ray beam perpendicular to the film surface (THROUGH) or parallel to the transverse direction (EDGE) (see Scheme 1) and by placing the film sample parallel to the axis of the cylindrical camera, are shown in Figure 1. The two patterns are identical and clearly indicate the presence of the trans-planar mesomorphic phase of s-PS,[21] with axial orientation. This mesomorphic phase is characterized by the presence of s-PS chains exhibiting trans-planar conformation, as clearly shown by the typical distance between the equator and the layer line (leading to chain periodicity $c = 0.51$ nm, see Figure 1) as well as by the corresponding FTIR spectra (not shown) presenting the typical H-chain wagging mode at 1223 cm^{-1},[22] which for amorphous samples is of much lower intensity and located at 1196 cm^{-1}.This axially oriented mesomorphic film, as a consequence of sorption of carbon disulfide (CS_2) and 1,4-dimethylnaphthalene (DMNP), cocrystallizes leading to clathrate and intercalate phases, respectively, exhibiting the helical s(2/1)2 conformation. These cocrystallizations with CS_2 and DMNP induce $a_{\parallel}c_{\parallel}$[6a,b,h] and $a_{\perp}c_{\parallel}$[6e,h] uniplanar orientations respectively, which adds to the starting axial orientation ($f_c^{IR} \approx 0.9$).

These two uniplanar−axial orientations have been achieved for cocrystalline phases presenting different guest molecules and have been also maintained as a consequence of guest−exchange procedures leading to cocrystalline phases including different guest molecules. For instance, both kind of orientations have been obtained for cocrystalline phases including DMNP.

An easier comparison between the two uniplanar−axial orientations can be obtained after procedures of guest removal, leading for both cocrystalline phases to the nanoporous δ form.[7] The photographic X-ray diffraction patterns of the two biaxially stretched films exhibiting the nanoporous δ form, as taken by having the X-ray beam perpendicular to the film surface (THROUGH) or parallel to the transverse direction (EDGE) or parallel to the main draw direction (END) (see Scheme 1) are shown in Figure 2. The EDGE and THROUGH patterns clearly indicate the occurrence of axial orientation with reflections organized in layer lines (with the typical chain periodicity $c = 0.78$ nm, see Figure 2). However, as also indicated in Table 1, the relative intensity of the peaks, are completely different for the THROUGH and EDGE patterns and clearly indicate the occurrence of two different uniplanar−axial orientation $a_{\parallel}c_{ax}$ and $a_{\perp}c_{ax}$, for the films crystallized by CS_2 and DMNP (lower and upper part of Figure 2, respectively). These kinds of orientation immediately allow to understand that the EDGE and THROUGH patterns of the film crystallized by CS_2 are strictly similar, respectively, to the THROUGH and EDGE patterns of the films crystallized by DMNP, respectively. Moreover, the occurrence of $a_{\parallel}c_{ax}$ and $a_{\perp}c_{ax}$ uniplanar−axial orientations allow to rationalize that the END patterns of the films are very similar but rotated of 90° (right part of Figure 2). The degree of uniplanar orientation (see Experimental Section) is close to 0.8 for both samples of Figure 2.

dx.doi.org/10.1021/ma200806x |*Macromolecules* 2011, 44, 5671–5681

Table 1. Relative Intensities of the Reflections of the δ Form for Films Exhibiting the Simple Axial Orientation or the $a_{\parallel}c_{ax}$ and $a_{\perp}c_{ax}$ Uniplanar−Axial Orientation (for THROUGH, EDGE, and END Patterns)[a]

	δ axial			δ uniplanar−axial				
				THROUGH $a_{\parallel}c_{ax}$ or EDGE $a_{\perp}c_{ax}$	EDGE $a_{\parallel}$ c_{ax} or THROUGH $a_{\perp}c_{ax}$	END		
hkl	$2\theta_{obs.}$	$2\theta_{calc.}$	$I_{obs.}$	$I_{obs.}$	$I_{obs.}$	$I_{obs.}$	χ $a_{\parallel}c_{ax}$	χ $a_{\perp}c_{ax}$
010	8.5	8.37	vs	w	vvs	vvs	0	90
$\bar{2}$10	10.2	10.65	vw	ms		m	75	15
200	11.5	11.41	vw					
$\bar{2}$20	15.0	15.43	w	vvw	mw		45	45
020	17.0	16.8	w	mw	vw	vw	0	90
210		16.99				m	40	50
$\bar{4}$10	20.75	20.51	w	mw	vvw	m	75	25
$\bar{4}$20		21.41						
101	13.35	12.84	vs	ms	ms			
$\bar{1}$11		13.85						
111	16.71	16.8	ms	w	vs			
211	20.7	20.56	s	vs	m			
301		20.7						
$\bar{3}$21		21.2						
$\bar{4}$11	23.5	23.57	s	ms	w			
$\bar{4}$21		24.37						

[a] For the END pattern the azimuthal angle of the observed reflection is also reported.

Table 2. Relative Intensities of the Reflections of the γ Form for Films Exhibiting the Simple Axial Orientation or the $a_{\parallel}c_{ax}$ and $a_{\perp}c_{ax}$ Uniplanar−Axial Orientation (for THROUGH, EDGE, and END Patterns)[a]

	γ axial			γ uniplanar−axial				
				THROUGH $a_{\parallel}c_{ax}$ or EDGE $a_{\perp}c_{ax}$	EDGE $a_{\parallel}$ c_{ax} or THROUGH $a_{\perp}c_{ax}$	END		
hkl	$2\theta_{obs.}$	$2\theta_{calc.}$	$I_{obs.}$	$I_{obs.}$	$I_{obs.}$	$I_{obs.}$	χ $a_{\parallel}c_{ax}$	χ $a_{\perp}c_{ax}$
010	5.25	5.23	w		m	mw	0	90
200	9.25	9.24	s	vs	vvw	vs	90	0
020	10.5	10.47	m	w	vs	vvs	0	90
210		10.62						
220	14.0	13.98	mw	w	w	m	45	45
030	15.75	15.74	mw	w	s	m	0	90
410	19.25	19.26	m	w	m	mw	70	20
040	21.25	21.02	mw	mv	m	m	0	90
420		21.33					60	30
240	23	23.01	w	vw	mw	w	15	75
121	16.25	16.04	vs	m	vvs			
031	19.94	19.35	s	vs	w			
131		19.90						
231	21.66	21.48	mw	s	m			
401		21.71						
041	23.81	23.88	mw	ms	vw			
331		23.89						

[a] For the END pattern the azimuthal angle of the observed reflection is also reported.

The annealing of both these films in restrained conditions followed by sorption and desorption of chloroform,[8] allows the achievement of γ and ε form films, which can retain essentially unaltered the degree of both axial and uniplanar orientations. In this respect, it is worth noting that, as γ form films with $a_{\parallel}c_{\parallel}$ and $a_{\perp}c_{\parallel}$ uniplanar orientations lead to ε form films with $a_{\perp}$ and $b_{\perp}$ uniplanar orientations,[6i] γ form films with $a_{\parallel}c_{ax}$ and $a_{\perp}c_{ax}$, uniplanar−axial orientations lead to ε form films with $a_{\perp}c_{ax}$ and $b_{\perp}c_{ax}$ uniplanar−axial orientations, respectively.

dx.doi.org/10.1021/ma200806x |*Macromolecules* 2011, 44, 5671–5681

Table 3. Relative Intensities of the Reflections of the ε Form for Films Exhibiting the Simple Axial Orientation or the $a_{\perp}c_{ax}$ and $b_{\perp}c_{ax}$ Uniplanar−Axial Orientation (for THROUGH, EDGE, and END Patterns)[a]

	ε axial			ε uniplanar−axial				
				THROUGH $a_{\perp}c_{ax}$ or EDGE $b_{\perp}c_{ax}$	EDGE $a_{\perp}c_{ax}$ or THROUGH $b_{\perp}c_{ax}$	END		
hkl	$2\theta_{obs.}$	$2\theta_{calc.}$	$I_{obs.}$	$I_{obs.}$	$I_{obs.}$	$I_{obs.}$	χ $a_{\perp}c_{ax}$	χ $b_{\perp}c_{ax}$
110	6.90	6.75	s	vw	vvs	vs	35	55
020	8.10	8.0	s	vvs	m	vs	90	0
220	13.8	13.6	m	w	m	mw	35	55
040	16.4	16.1	w	vvw	mw	w	90	0
330	20.4	20.2	m	w	mw	mw	35	55
420	22.3	23.4	m	vvw	mw	mw	20	70
111	13.2	13.0	w	vw	vw			
021		13.8						
211	16.1	16.1	vs	ms	vvs			
131		17.4						
221		17.7						
041	20.2	19.7	vs	vvs	ms			
231		19.7						
311		20.2						
141		20.2						
331	23.5	23.4	m	ms	vw			
115		24.0						

[a] For the END pattern the azimuthal angle of the observed reflection is also reported.

The strict similarity between EDGE and THROUGH patterns of films with opposite orientation of the *a* axis, above-described for the δ form films, is maintained also for γ and ε films. As a consequence, for the sake of simplicity, only the X-ray diffraction patterns of films exhibiting the $a_{\parallel}c_{ax}$ uniplanar−axial orientation for the γ form and the corresponding $a_{\perp}c_{ax}$ uniplanar−axial orientation for the ε form, are shown in Figure 3 (upper and lower part, respectively). The relative intensities of the reflections of the γ and ε form films of Figure 3 are listed in Tables 2 and 3, respectively. It is worth noting that the reflections in both THROUGH and EDGE patterns of γ and ε form films (Figure 3) are narrower than those observed for the starting δ form films (Figure 2). This phenomenon could erroneously suggest the occurrence of an unexpected increase of orientational order, associated with the thermal treatment leading to the $\delta \rightarrow \gamma$ transition. The phenomenon is instead more simply explained by the transition from the monoclinic δ phase toward the orthorhombic γ and ε phases. In fact, for an ideal uniplanar−axial orientation, crystallites with orthorhombic unit cell all present an identical three-dimensional orientation in the film while crystallites with monoclinic unit cell are divided in two sets exhibiting two slightly different orientations (associated with the opposite directions of the *c* axis of the unit cell with respect to the main draw direction). In this respect, it is worth adding that the high degree of uniplanar orientation is essentially maintained for the γ films, as clearly shown by the large differences between THROUGH and EDGE patterns of Figure 3; moreover, data collected in Table 2 could be helpful for the resolution of the crystal structure of the γ phase,[8] which is still unknown.

In the conclusion of this section, a schematic representation of the processing methods inducing two different uniplanar−axial orientations for the nanoporous δ and ε phases in s-PS films is reported (Figure 4). Depending on the guest used to recrystallize the biaxially stretched mesomorphic films, $a_{\parallel}c_{ax}$ and $a_{\perp}c_{ax}$ uniplanar−axial orientations in δ form films are obtained. The $a_{\parallel}c_{ax}$ and $a_{\perp}c_{ax}$ uniplanar−axial orientations of δ form films are transformed, after thermal treatment and subsequent sorption and desorption of chloroform, in the $a_{\perp}c_{ax}$ and $b_{\perp}c_{ax}$ orientations for ε form films, respectively.

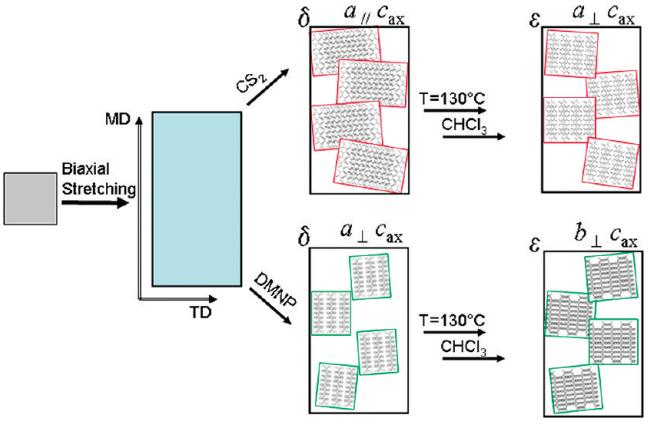

Figure 4. Schematic representation of the possible procedures inducing two different uniplanar−axial orientations for the nanoporous δ and ε phases in s-PS films. MD is the main draw direction, and TD is the transverse draw direction. For all films, the chain axes are preferentially parallel to MD (c_{ax}). Depending on the guest used to recrystallize the biaxially stretched mesomorphic films, $a_{\parallel}c_{ax}$ and $a_{\perp}c_{ax}$ uniplanar−axial orientations are obtained. The $a_{\parallel}c_{ax}$ and $a_{\perp}c_{ax}$ uniplanar−axial orientations of δ form films are transformed, after thermal treatment and subsequent sorption and desorption of chloroform, in the $a_{\perp}c_{ax}$ and $b_{\perp}c_{ax}$ orientations for ε form films, respectively.

dx.doi.org/10.1021/ma200806x |*Macromolecules* 2011, 44, 5671–5681

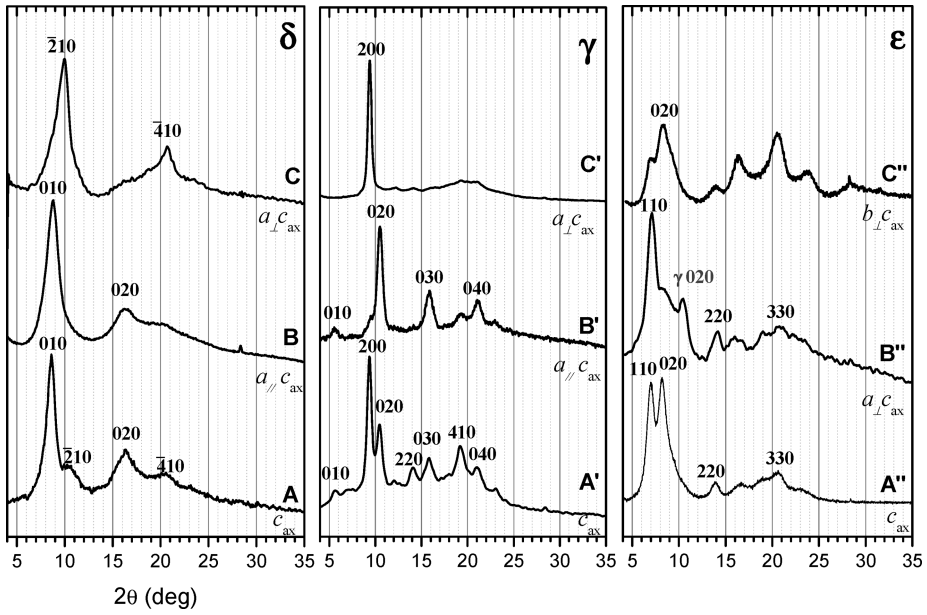

Figure 5. X-ray diffraction patterns, as taken by an automatic powder diffractometer, of δ, γ and ε form films: (A, A′, and A″) simple c−axial orientation; (B and B′) $a_{||}c_{ax}$ orientation of δ and γ phases and (B″) the derived $a_\perp c_{ax}$ orientation of ε phase; (C and C′) $a_\perp c_{ax}$ orientation of δ and γ phases and (C″) the derived $b_\perp c_{ax}$ orientation of ε phase. The Miller indexes of the main reflections have been indicated.

As already discussed for films exhibiting different uniplanar orientations,[6i] the two different uniplanar−axial orientations lead to completely different orientations of the cavity and channels of the δ and ε nanoporous crystalline phases and hence of the relative guest molecules. Moreover, already on inspection of Figure 4, it is apparent that, for the δ phase, the $a_\perp c_{ax}$ uniplanar−axial orientation presents higher guest diffusivities than the $a_{||}c_{ax}$ uniplanar−axial orientation. In this respect, it is worth adding that the analogous higher guest diffusivity of δ form films with $a_\perp c_{||}$ with respect to those with $a_{||}c_{||}$ uniplanar orientation has been already predicted[17a] and experimentally proved for many guest molecules.[17b−d]

X-ray Diffraction Patterns, Taken with an Automatic Powder Diffractometer, of Films Presenting Uniplanar−Axial Orientations of Their Crystalline Phases. In this section, X-ray diffraction patterns of films presenting the two different kinds of uniplanar−axial orientations of δ, γ, and ε phases, as collected by an automatic powder diffractometer, i.e., with the technique most frequently used in the majority of laboratories, are compared with those of films simply exhibiting the axial orientation. The main aim is to facilitate the recognition of the possible occurrence and of the kind of uniplanar−axial orientation in s-PS films, by using simple and rapidly achieved diffraction measurements.

In Figure 5, the X-ray diffraction patterns of δ, γ and ε form films exhibiting the simple c-axial orientation (A, A′, and A″) or the two different kinds of uniplanar−axial orientations, $a_{||}c_{ax}$ for δ and γ phases (B and B′) and the derived $a_\perp c_{ax}$ orientation for ε phase (B″) and $a_\perp c_{ax}$ orientation for δ and γ phases (C and C′) and the derived $b_\perp c_{ax}$ orientation for ε phase (C″) are compared. The films of Figures 5B,C are the same films used for the characterization studies of Figures 2 and 3.

As usual for axial orientations, the patterns of Figure 5, parts A, A′, and A″, show increased intensity of the equatorial reflections, i.e., of those with $hk0$ Miller indexes. Of course, the patterns of the films exhibiting uniplanar−axial orientation maintain these features, while the relative intensities of the equatorial reflections are drastically changed. In particular, the $a_{||}c_{ax}$ and the $a_\perp c_{ax}$ uniplanar−axial orientations maximizes and minimize the $0k0$ reflections, respectively.

Influence of the Guest on the Kind of Uniplanar−Axial Orientation of δ Cocrystalline Phases. Recent studies have shown that guest-induced crystallizations in amorphous s-PS films[6g] lead to host−guest δ cocrystalline phases always exhibiting uniplanar orientation. In particular, depending on the used guest, $a_{||}c_\perp$[6d,h] or $a_\perp c_{||}$[6e,h] uniplanar orientations can be induced, thus leading to crystalline chain axes preferentially perpendicular or parallel to the film plane, respectively. All of these cocrystalline phases, after guest removal, lead to the nanoporous δ phase always maintaining the initial uniplanar orientation. Information on the kind of uniplanar orientation as induced in amorphous s-PS films, taken from ref 6g, is collected in the sixth column of Table 4.

Information on the kind of orientation, as induced in biaxially and uniaxially stretched trans-planar mesomorphic s-PS films (like those of Figure 1) by the same guests,is collected in the columns 7 and 8 of Table 4. Independently of the guest choice, all these samples present the c axis parallel to the main draw direction (c_{ax}). This, of course, is due to the prevalence of the orientation imposed by the stretching with respect to the orientation imposed by the guest-induced crystallization. As for the a axis, less volatile guests (exhibiting slower diffusivities and cocrystallization kinetics in s-PS) produce $a_\perp$ orientation, as already observed for the crystallization induced in amorphous s-PS films (ref 6g and column 6 in Table 4). However, for stretched films (mainly for uniaxially stretched) the $a_\perp$ orientation is already induced by guests exhibiting much higher volatility (columns 7 and 8 in Table 4). More volatile guests, exhibiting high cocrystallization kinetics in s-PS, induce uniplanar orientation (in particular, the $a_{||}$ orientation) only in amorphous or biaxially stretched films. Hence, guests inducing fast s-PS cocrystallization also induce $a_{||}c_{ax}$ uniplanar−axial orientation in

dx.doi.org/10.1021/ma200806x |Macromolecules 2011, 44, 5671–5681

Table 4. Kinds of Orientations of δ Co-Crystalline Phases (and Derived Nanoporous δ Phases), Which Are Obtained by Room Temperature Co-Crystallization As Induced by the Listed Guests, in Unoriented Amorphous and Biaxially and Uniaxially Stretched Mesomorphic s-PS Films, Respectively[a]

guest					solvent-induced orientation in films		
name	formula	co-crystallization Kinetic index I_C	Bp (°C)	Vp (mm Hg @ 20 °C)	unoriented amorphous[b]	biaxially stretched, trans-planar mesomorphic	monoaxially stretched, trans-planar mesomorphic
chloroform	$CHCl_3$	1	61	160	$a_{\parallel}c_{\perp}$	$a_{\parallel}c_{ax}$	c_{ax}
dichloromethane	CH_2Cl_2	0.7	40	349	$a_{\parallel}c_{\perp}$	$a_{\parallel}c_{ax}$	c_{ax}
carbon disulfide	CS_2	_	46	297	$a_{\parallel}c_{\perp}$	$a_{\parallel}c_{ax}$	c_{ax}
tetrahydrofuran	C_4H_8O	0.5	66	129	$a_{\parallel}c_{\perp}$	$a_{\parallel}c_{ax}$	$a_{\perp}c_{ax}$
trichloroethylene	$Cl_2C{=}CHCl$	0.3	87	61	$a_{\parallel}c_{\perp}$	$a_{\parallel}c_{ax}$	$a_{\perp}c_{ax}$
benzene	C_6H_6	0	80	75	$a_{\parallel}c_{\perp}$	$a_{\perp}c_{ax}$	$a_{\perp}c_{ax}$
1,2-dichloroethane	$ClCH_2CH_2Cl$	0	83	64	$a_{\parallel}c_{\perp}$	$a_{\perp}c_{ax}$	$a_{\perp}c_{ax}$
1,2-dichloropropane	$CH_3CHClCH_2Cl$	0	95−96	40	$a_{\parallel}c_{\perp}$	$a_{\perp}c_{ax}$	_
toluene	$C_6H_5CH_3$	0	110−111	21	$a_{\parallel}c_{\perp}$	$a_{\perp}c_{ax}$	$a_{\perp}c_{ax}$
o-xylene	*o*-$C_6H_4(CH_3)_2$	0	144	7	$a_{\perp}c_{\parallel}$	$a_{\perp}c_{ax}$	_
decahydronaphthalene	$C_{10}H_{18}$	_	190	42[d]	$a_{\perp}c_{\parallel}$	_	_
1,4-dimethylnaphthalene	$C_{10}H_6(CH_3)_2$	_	262[c]	0.004	$a_{\perp}c_{\parallel}$	$a_{\perp}c_{ax}$	_

[a] Bp is the boiling point at atmospheric pressure, and Vp is the vapor pressure at 20 °C. The last three columns contain the orientation of the δ cocrystalline phases and of the corresponding empty δ phases. [b] Data from ref 6g. [c] At 751 mmHg. [d] At 92 °C.

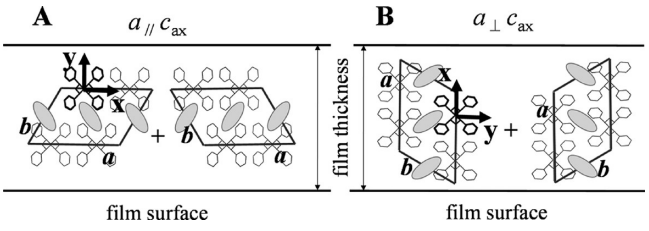

Figure 6. Along the chain axis representation of the two possible orientations of the monoclinic unit cell of the δ form of s-PS with respect to the film surface for the ideal $a_{\parallel}c_{ax}$ (A) and $a_{\perp}c_{ax}$ (B) uniplanar−axial orientations. Symmetry considerations relative to the s(2/1)2 helical chains impose that TMV have to be parallel or perpendicular to the chain axis and that those perpendicular have to be along the binary axes, indicated by *x* and *y*. In particular, the *x* and *y* binary axes of the s(2/1)2 helices pass through the external or internal methylenes[12b] and are parallel and perpendicular to the *a* axis of the monoclinic unit cell of the δ phase.[7a]

biaxially stretched films (column 7 of Table 4) while, as generally occurs for polymers, simply induce the axial (c_{ax}) orientation in uniaxially stretched films (column 8 of Table 4).

In summary, our results indicate that, when the rate of advancement of the guest front is slow or fast, the cocrystallization process occurs with the *a* axis (i.e., the direction of closest packing of polymer helices) perpendicular or parallel to the advancing front (and to the film surface), as shown in Figure 6, parts A and B, respectively.

Characterization of Films with $a_{\parallel}c_{ax}$ and $a_{\perp}c_{ax}$ Uniplanar−Axial Orientations by Polarized FTIR Spectra. For films exhibiting the two different uniplanar−axial orientations, also informative are the Fourier Transform Infrared (FTIR) spectra, as obtained by placing the film perpendicular to the polarized light, with polarization plane parallel or perpendicular to the *c* axis. For instance, the polarized FTIR spectra of the δ and γ form films of Figures 2 and 3, exhibiting $a_{\parallel}c_{ax}$ and $a_{\perp}c_{ax}$ orientations, are shown in Figure 7. In particular, spectra collected with polarization plane parallel and perpendicular to the *c* axis are shown in Figure 7, parts A−A′ and B−B′, respectively.

The spectra obtained for *polarization plane parallel to the main draw direction* (Figure 7A−A′) are very similar for the two films with different orientations. In fact, these spectra maximize the intensity of the peaks whose transition moment vectors (TMV) are parallel to the draw direction. Because the two films with different uniplanar−axial orientation exhibit the same axial orientation, i.e., the polymer chain axis (*c*-axis) parallel to the main draw direction, both spectra show maximum absorbance for peaks whose TMV are parallel to the polymer chain axis (z), as, e.g., those at 1354, 1276, 944, 572, and 535 cm^{-1}.[12b] More informative are the spectra obtained for *polarization plane perpendicular to the main draw direction* (Figure 7B−B′), being definitely different for the two films. In fact, as shown for the δ phase[7a] in Figure 6, films with $a_{\parallel}c_{ax}$ (Figure 6A) and $a_{\perp}c_{ax}$ (Figure 6B) orientations present the *x* and *y* binary axes (which pass through the external and internal methylene groups of the s(2/1)2 polymer helices) in the film plane and parallel to the polarization plane. As a consequence, for film with $a_{\parallel}c_{ax}$ and $a_{\perp}c_{ax}$ uniplanar−axial orientations, the peaks whose TMV are parallel to the *x*-axis (like those at 1320, 934, 778, 601, and 503 cm^{-1}, thick lines in Figure 7B)[12b] or to the *y* axis (like those at 1378, 1169, 608, and 581 cm^{-1}, thin lines in Figure 7B)[12b] are maximized, respectively.

It is worth adding that the FTIR polarized spectra of films with the δ form (Figure 7B) and of the derived γ (Figure 7B′) and ε the form (not reported), exhibit similar absorbance differences associated with the two different uniplanar−axial orientations. This demonstrates that, along the δ → γ → ε transitions, the s(2/1)2 helices of the s-PS crystalline phases maintain not only their axial orientation but also their in plane orientation, i.e., *x* or *y* axes of the helices remain parallel to the film surface. As for δ[7a] and ε[9c] forms, the present information based on polarized FTIR spectra of films exhibiting two different uniplanar−axial orientations, has been independently obtained by X-ray diffraction data.[6i] In particular, the maintenance of uniplanar orientation

dx.doi.org/10.1021/ma200806x |*Macromolecules* 2011, 44, 5671–5681

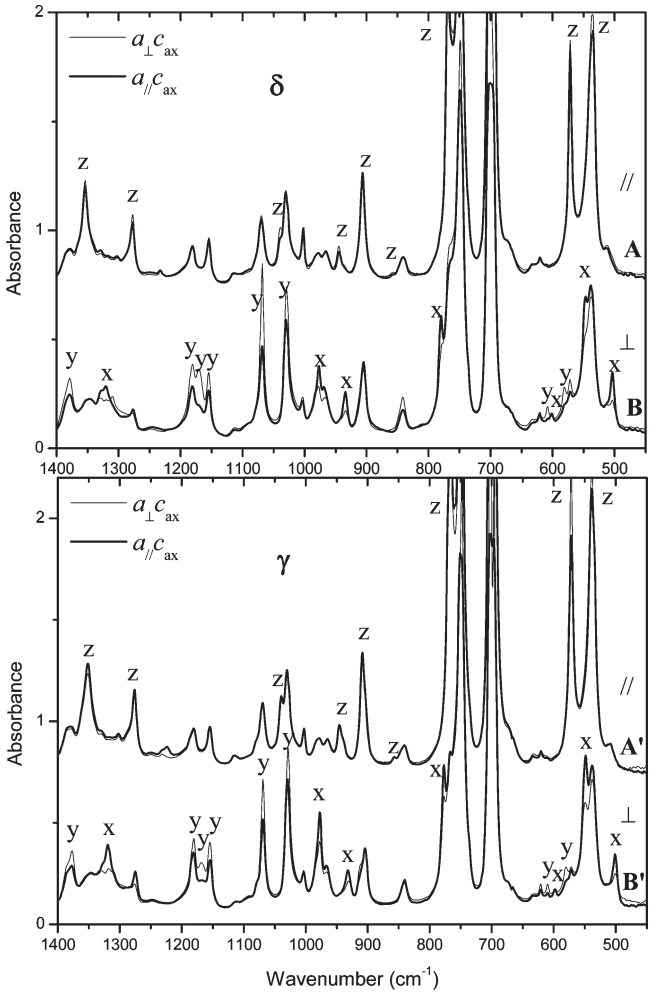

Figure 7. FTIR spectra, as collected with polarization plane parallel (A, A′) and perpendicular (B, B′) to the *c* axis, of δ and γ form films exhibiting different uniplanar−axial orientations. In A and A′, both uniplanar−axial orientations maximize, absorbance peaks corresponding to TMV parallel to the polymer chain axis (*z*). In B and B′, $a_{||}c_{ax}$ (thick lines) and $a_\perp c_{ax}$ (thin lines) uniplanar−axial orientations maximize, absorbance peaks corresponding to TMV that are along the *x* and *y* axes, respectively (see Figure 6).

($a_{||}c_{||}$ and $a_\perp c_{||}$ for the δ phase become $a_\perp$ and $b_\perp$ for the ε phase) combined with the precise knowledge of their crystal structures, clearly indicate the maintenance of the in-plane orientation for all crystalline helices (compare parts A and C of Figure 8).

In this respect, it is worth adding that polarized FTIR spectra like those of Figure 7 give a relevant insight relative to the still unknown crystal structure of the γ phase. In fact, as schematically shown in Figure 8B, the δ → γ transition, which occurs with maintenance of the $a_{||}c_{||}$ (or of the $a_\perp c_{||}$) orientation,[6h] also occurs with maintenance of the in-plane orientation of all the helices. The schematic model of the γ form of Figure 8B also assumes alternation between *R* and *L* helices, along the *x*-direction, because it is present in the precursor δ form (Figure 8A) and it is maintained also in derived ε form (Figure 8C). Of course, for a complete definition of the γ form crystal structure, relative shifts (along *a* and *c*) of layers of alternated enantiomorphous helices have still to be defined.

CONCLUSIONS

Uniaxial and unbalanced biaxial stretching procedures on amorphous s-PS films lead to the formation of axially oriented trans-planar mesomorphic phases. Starting from these films, guest-induced cocrystallization procedures, by suitable selection of the low-molecular-mass guest molecules, can lead to two different kinds of uniplanar−axial orientations, both exhibiting the polymer chain axis (*c*-axis) parallel to the main draw direction while a different crystal plane presents a preferential orientation with respect to the film plane. The two obtained uniplanar−axial orientations, which correspond to the combination of the *c*-axial orientation with the $a_{||}c_{||}$ and $a_\perp c_{||}$ uniplanar orientations,[6] are more simply defined as $a_{||}c_{ax}$ and $a_\perp c_{ax}$ uniplanar−axial orientations, where ax indicates parallel to the main draw direction while || and ⊥ indicate parallel and perpendicular to the film plane.

Both kinds of uniplanar−axial orientations can be maintained after solvent-exchange procedures leading to cocrystalline phases with different guests, after guest extraction procedures leading to the monoclinic nanoporous δ phase, after the thermal treatments leading to the orthorhombic γ phase as well as after the chloroform sorption−desorption procedures leading to the orthorhombic nanoporous ε phase. In particular, the $a_{||}c_{ax}$ and $a_\perp c_{ax}$ uniplanar−axial orientations

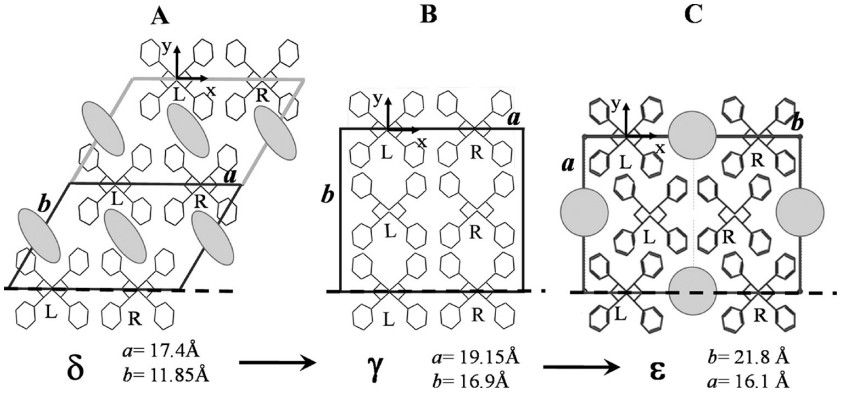

Figure 8. Maintenance of the same in-plane and axial orientation for all the helices of the unit cell, during the δ → γ → ε transitions. The unit cell of the δ[7a] (A) and ε[9c] (C) phases are those described in the literature while the packing of the γ phase is schematically sketched (B), on the basis of the polarized FTIR data of this paper (relative shifts, along *a* and *c*, of structural layers of alternated enantiomorphous helices have still to be defined).

dx.doi.org/10.1021/ma200806x |*Macromolecules* 2011, 44, 5671–5681

of the native cocrystalline films are maintained in the δ and γ form films and transformed in the $a_{\perp}c_{ax}$ and $b_{\perp}c_{ax}$ orientations respectively, for the ε form films (Figure 4).

A detailed study on the different kinds of orientations, which are induced in s-PS uniaxially and biaxially stretched trans-planar mesomorphic films by many different guest molecules, has allowed to establish that, independently of the guest choice, all these samples present the *c* axis parallel to the draw direction (c_{ax}). As for the *a* axis, less and more volatile guests, inducing slow and fast cocrystallization kinetics in s-PS, induce on biaxially stretched films *a* axis orientation perpendicular and parallel to the film plane ($a_{\perp}$ and $a_{\parallel}$), respectively. This indicates that, when the rate of advancement of the guest front is slow or fast, the cocrystallization process occurs with the *a* axis (i.e., the direction of closest packing of polymer helices) perpendicular or parallel to the advancing front (and to the film surface), respectively.

For films exhibiting the two different uniplanar−axial orientations, also informative are the Fourier Transform Infrared (FTIR) spectra. Particularly informative are the spectra obtained for polarization plane perpendicular to the main draw direction, being definitely different for the two uniplanar−axial orientations. For δ form films with $a_{\parallel}c_{ax}$ and $a_{\perp}c_{ax}$ uniplanar−axial orientation the peaks whose TMV are parallel to the binary axes (perpendicular to the chain axis) passing through the external methylene groups (*x*-axis of Figure 6, like peaks at 1320, 934, 778, 601, and 503 cm^{-1})[12b] or through the internal methylene groups (*y* axis of Figure 6, like peaks at 1378, 1169, 608, and 581 cm^{-1})[12b] are maximized, respectively. Polarized FTIR spectra of the films with uniplanar−axial orientation have also allowed establishing the orientation of all s(2/1)2 helices with respect to the unit cell axes of γ form, thus giving a relevant contribution to the definition of its still unknown crystalline structure.

The described processing methods make available polymer films with the highest possible level of orientational order. The achievement of a maximum level of orientation between the crystallites in the polymer films can be particularly relevant for the cocrystalline phases with active guest molecules. In fact, the level of 3-D orientational order in a flexible polymer film becomes close to that one of single crystals and the anisotropy of the optical,[14] electric,[15] or magnetic[16] properties can be maximized.

AUTHOR INFORMATION

Corresponding Author

*Telephone: +39 (0) 89 969582. Fax: +39 (0) 89 969603; E-mail: prizzo@unisa.it.

ACKNOWLEDGMENT

We thank Prof. Vincenzo Venditto, Dr. C. D'Aniello, and A. De Girolamo del Mauro of University of Salerno, for useful discussions. Financial support of the "Ministero dell'Istruzione, dell'Università e della Ricerca" (PRIN2007), and of the Consortium INSTM (PRISMA project) is gratefully acknowledged.

REFERENCES

(1) (a) Heffelfinger, C. J.; Burton, R. L. *J. Polym. Sci.* **1960**, *47*, 289–306.(b) Werner, E.; Janocha, S.; Hopper, M. J.; Mackenzie In *Encyclopedia of Polymer Science and Engineering*, 2nd ed.; Wiley-Interscience: New York, 1986; Vol. 12 p 193.

(2) Gohil, R. M. *J. Appl. Polym. Sci.* **1993**, *48*, 1649–1664.

(3) (a) Uejo, H.; Hoshino, S. *J. Appl. Polym. Sci.* **1970**, *14*, 317–328. (b) Bartczak, Z.; Martuscelli, E. *Polymer* **1997**, *38*, 4139–49. (c) Saraf, R. F. *Polymer* **1994**, *35*, 1359–1368. (d) Rizzo, P.; Venditto, V.; Guerra, G.; Vecchione, A. *Macromol. Symp.* **2002**, *185*, 53–63. (e) Rizzo, P.; Albunia, A. R. *Macromol. Chem. Phys.* **2011**, *212*, 10.1002/macp.201100036.

(4) Natta, G.; Corradini, P. *Nuovo Cimento Suppl.* **1960**, *15*, 40–51.

(5) (a) Chatani, Y.; Inagaki, T.; Shimane, Y.; Ijitsu, T.; Yukimori, T.; Shikuma, H. *Polymer* **1993**, *34*, 1620–1624. (b) Chatani, Y.; Shimane, Y.; Inagaki, T.; Shikuma, H. *Polymer* **1993**, *34*, 4841–4845. (c) De Rosa, C.; Rizzo, P.; Ruiz de Ballesteros, O.; Petraccone, V.; Guerra, G. *Polymer* **1999**, *40*, 2103–2110. (d) Petraccone, V.; Tarallo, O.; Venditto, V.; Guerra, G. *Macromolecules* **2005**, *38*, 6965–6971. (e) Musto, P.; Rizzo, P.; Guerra, G. *Macromolecules* **2005**, *38*, 6079–6089. (f) Tarallo, O.; Petraccone, V.; Venditto, V.; Guerra, G. *Polymer* **2006**, *47*, 2402–2410. (g) Tarallo, O.; Schiavone, M. M.; Petraccone, V.; Daniel, C.; Rizzo, P.; Guerra, G. *Macromolecules* **2010**, *43*, 1455–1466. (h) Tarallo, O.; Petraccone, V.; Albunia, A. R.; Daniel, C.; Guerra, G. *Macromolecules* **2010**, *43*, 8549–8558.

(6) (a) Rizzo, P.; Albunia, A. R.; Milano, G.; Venditto, V.; Guerra, G.; Mensitieri, G.; Di Maio, L. *Macromol. Symp.* **2002**, *185*, 65–75. (b) Rizzo, P.; Lamberti, M.; Albunia, A. R.; Ruiz de Ballesteros, O.; Guerra, G. *Macromolecules* **2002**, *35*, 5854–5860. (c) Rizzo, P.; Costabile, A.; Guerra, G. *Macromolecules* **2004**, *37*, 3071–3076. (d) Rizzo, P.; Della Guardia, S.; Guerra, G. *Macromolecules* **2004**, *37*, 8043–8049. (e) Rizzo, P.; Spatola, A.; De Girolamo Del Mauro, A.; Guerra, G. *Macromolecules* **2005**, *38*, 10089–10094. (f) Daniel, C.; Avallone, A.; Rizzo, P.; Guerra, G. *Macromolecules* **2006**, *39*, 4820–4823. (g) Albunia, A. R.; Annunziata, L.; Guerra, G. *Macromolecules* **2008**, *41*, 2683–2688. (h) Albunia, A. R.; Rizzo, P.; Tarallo, O.; Petraccone, V.; Guerra, G. *Macromolecules* **2008**, *41*, 8632–8642. (i) Albunia, A. R.; Rizzo, P.; Guerra, G. *Chem. Mater.* **2009**, *21*, 3370–3375.

(7) (a) De Rosa, C.; Guerra, G.; Petraccone, V.; Pirozzi, B. *Macromolecules* **1997**, *30*, 4147–4152. (b) Milano, G.; Venditto, V.; Guerra, G.; Cavallo, L.; Ciambelli, P.; Sannino, D. *Chem. Mater.* **2001**, *13*, 1506–1511. (c) Gowd, E. B.; Shibayama, N.; Tashiro, K. *Macromolecules* **2006**, *39*, 8412–8418.

(8) (a) Immirzi, A.; de Candia, F.; Iannelli, P.; Zambelli, A.; Vittoria, V. *Makromol. Chem., Rapid Commun.* **1988**, *9*, 761–764. (b) Tamai, Y.; Fukuda, M. *Macromol. Rapid Commun.* **2002**, *23*, 892–895. (c) Rizzo, P.; Albunia, A. R.; Guerra, G. *Polymer* **2005**, *46*, 9549–9554.

(9) (a) Rizzo, P.; Daniel, C.; De Girolamo Del Mauro, A.; Guerra, G. *Chem. Mater.* **2007**, *19*, 3864–3866. (b) Rizzo, P.; D'Aniello, C.; De Girolamo Del Mauro, A.; Guerra, G. *Macromolecules* **2007**, *40*, 9470–9474. (c) Petraccone, V.; Ruiz de Ballesteros, O.; Tarallo, O.; Rizzo, P.; Guerra, G. *Chem. Mater.* **2008**, *20*, 3663–3668.

(10) (a) De Rosa, C.; Guerra, G.; Petraccone, V.; Corradini, P. *Polym. J.* **1991**, *23*, 1435–1442. (b) Cartier, L.; Okihara, T.; Lotz, B. *Macromolecules* **1998**, *31*, 3303–3310.

(11) (a) De Rosa, C.; Rapacciuolo, M.; Guerra, G.; Petraccone, V.; Corradini, P. *Polymer* **1992**, *33*, 1423–1428. (b) Chatani, Y.; Shimane, Y.; Ijitsu, T.; Yukinari, T. *Polymer* **1993**, *34*, 1625–1629.

(12) (a) Albunia, A. R.; Rizzo, P.; Guerra, G.; Torres, F. J.; Civalleri, B.; Zicovich-Wilson, C. M. *Macromolecules* **2007**, *40*, 3895–3897. (b) Torres, F. J.; Civalleri, B.; Meyer, A.; Musto, P.; Albunia, A. R.; Rizzo, P.; Guerra, G. *J. Phys. Chem.* **2009**, *113*, 5059–5071.

(13) (a) Albunia, A. R.; Di Masi, S.; Rizzo, P.; Milano, G.; Musto, P.; Guerra, G. *Macromolecules* **2003**, *36*, 8695–8603. (b) Albunia, A. R.; Milano, G.; Venditto, V.; Guerra, G. *J. Am. Chem. Soc.* **2005**, *127*, 13114–13115. (c) Itagaki, H.; Sago, T.; Uematsu, M.; Yoshioka, G.; Correa, A.; Venditto, V.; Guerra, G. *Macromolecules* **2008**, *41*, 9156–9164. (d) Albunia, A. R.; Graf, R.; Grassi, A.; Guerra, G.; Spiess, H. W. *Macromolecules* **2009**, *42*, 4929–4931. (e) Albunia, A. R.; Oliva, P.; Grassi, A. *J. Phys. Chem. A* **2011**, *115*, 443–452.

(14) (a) Venditto, V.; Milano, G.; De Girolamo Del Mauro, A.; Guerra, G.; Mochizuki, J.; Itagaki, H. *Macromolecules* **2005**, *38*, 3696–3702. (b) Stegmaier, P.; De Girolamo Del Mauro, A.; Venditto, V.; Guerra, G. *Adv. Mater.* **2005**, *17*, 1166–1168. (c) Uda, Y.; Kaneko, F.; Tanigaki, N.; Kawaguchi, T. *Adv. Mater.* **2005**, *17*, 1846–1850.

(d) D'Aniello, C.; Musto, P.; Venditto, V.; Guerra, G. *J. Mater. Chem.* **2007**, *17*, 531–535. (e) De Girolamo Del Mauro, A.; Carotenuto, M.; Venditto, V.; Petraccone, V.; Scoponi, M.; Guerra, G. *Chem. Mater.* **2007**, *19*, 6041–6046.

(15) (a) Daniel, C.; Galdi, N.; Montefusco, T.; Guerra, G. *Chem. Mater.* **2007**, *19*, 3302–3308.

(16) (a) Kaneko, F.; Uda, Y.; Kajiwara, A.; Tanigaki, N. *Macromol. Rapid Commun.* **2006**, *27*, 1643–1647. (b) Albunia, A. R.; D'Aniello, C.; Guerra, G.; Gatteschi, D.; Mannini, M.; Sorace, L. *Chem. Mater.* **2009**, *21*, 4750–4752. (c) Albunia, A. R.; D'Aniello, C.; Guerra, G. *Cryst. Eng. Commun.* **2010**, *12*, 3942–3949.

(17) (a) Milano, G.; Guerra, G.; Müller-Plathe, F. *Chem. Mater.* **2002**, *14*, 2977–2998. (b) Venditto, V.; De Girolamo Del Mauro, A.; Mensitieri, G.; Milano, G.; Musto, P.; Rizzo, P.; Guerra, G. *Chem. Mater.* **2006**, *18*, 2205–2510. (c) Annunziata, L.; Albunia, A. R.; Venditto, V.; Guerra, G. *Macromolecules* **2006**, *39*, 9166–9170. (d) Albunia, A. R.; Minucci, T.; Guerra, G. *J. Mater. Chem.* **2008**, *18*, 1046–1050.

(18) Albunia, A. R.; Musto, P.; Guerra, G. *Polymer* **2006**, *47*, 234–242.

(19) (a) Wilchinsky, Z. W. In *Advances in X-ray analysis*: Plenum Press: New York, 1963; Vol. 6, p 231. (b) Alexander, L. E. In *X-Ray Diffraction Methods in Polymer Science*; Krieger, R. E., Ed.; Hundington: New York, 1979; Chapter 4, p210.

(20) (a) Read, B. E. In *Structure and Properties of Oriented Polymers*; Ward, I. M., Ed.; London, 1975, Chapter 4; (b) Jasse, B.; Koenig, J. L. *J. Macromol. Sci. Rev. Macromol. Chem.* **1979**, *17*, 61–135.

(21) (a) De Candia, F.; Ruvolo, A.; Vittoria, V. *Makromol. Chem. Rapid. Commun.* **1991**, *12*, 295–299. (b) Petraccone, V.; Auriemma, F.; Dal Poggetto, F.; De Rosa, C.; Guerra, G.; Corradini, P. *Makromol Chem* **1993**, *194*, 1335–1345. (c) Auriemma, F.; Petraccone, V.; Dal Poggetto, F.; De Rosa, C.; Guerra, G.; Manfredi, C.; Corradini, P. *Macromolecules* **1993**, *26*, 3772–3777.

(22) Torres, F. J.; Civalleri, B.; Pisani, C.; Musto, P.; Albunia, A. R.; Guerra, G. *J. Phys. Chem. B.* **2007**, *111*, 6327–6335.